

Supplementary Material

Mechanisms behind excitation and concentration dependent multicolor photoluminescence in graphene quantum dots

Shuangquan Lai,^{a,b} Yong Jin,^{*a,b} Liangjie Shi,^{a,b} Rong Zhou,^{a,b} Yutang Zhou^{a,b} and
Dexin An^{a,b}

^a Key Laboratory of Leather Chemistry and Engineering, Ministry of Education,
Sichuan University, Chengdu 610065, P. R. China

^b National Engineering Laboratory for Clean Technology of Leather Manufacture,
Sichuan University, Chengdu 610065, P. R. China

Corresponding Author

*E-mail: jinyong@cioc.ac.cn

Experimental section

Preparation of graphene oxide (GO)

GO was prepared from natural graphite by using a modified version of Hummers' method. In the experiment, graphite (1.0 g), concentrated H₂SO₄ (25 mL), and a magnetic stirring bar were mixed in a 100 mL flask and sonicated (120 W) for 3 h at room temperature. Then, the equipment was magnetically stirred in an ice bath, then KMnO₄ (3.0 g) was slowly added to keep the temperature below 10 °C. Successively, the equipment was transferred to ultrasonic bath again and sonicated for another 3 h to obtain a dark green solution. Next, ultrapure water (15 mL) was slowly added, turning the color of the mixture to brown yellow. Additional ultrapure water (30 mL) was added and followed by addition of H₂O₂ (30%, 5 mL), turning the color of the mixture to bright yellow. Finally, the product was centrifuged and washed with HCl (1M) for 3 times. The obtained dispersion was purified by dialysis for one week using a dialysis membrane with a molecular weight cutoff of 5000 Da, and GO powder was obtained by lyophilization.

Morphological and Structural characteristics of GQDs

Fig. S1a displays the SEM image of GO, two-dimensional GO sheets with micron scale were found, and these GO sheets showed a curled morphology. Fig. S1b presents the TEM image of GO, the GO sheets in TEM image were found to be transparent. Fig. S1c shows the AFM image of GO, the GO sheets were also found to have micron scale lateral size with thickness of ca. 1 nm measured from the height profile of AFM image, illustrating that GO sheets have single atomic layered structure. The results demonstrated that the treatment of graphite with the modified Hummer's method resulted in the production of single layer GO sheets. Insights into the morphology of the as-prepared GQDs were also obtained from the SEM (Fig. S1d), TEM (Fig. S1e) and AFM (Fig. S1f) measurements. From SEM image, large amount of aggregated GQDs with roundish morphology and diameter ranging from 40 nm to 120 nm can be observed, which can be in sharp contrast to that of GO. From TEM image, it can be seen that the obtained GQDs have diameters of ca. 40-80 nm, and stacked roundish GQDs can be observed. The thickness of GQDs was measured by AFM characterization. The height of the GQDs was ca. 1-2 nm as shown in the height profile of AFM image, higher thickness than that of single layered GO is due to the stacking of GQDs as shown in TEM image, which is clear illustration of a single atomic layer structure of GQDs.

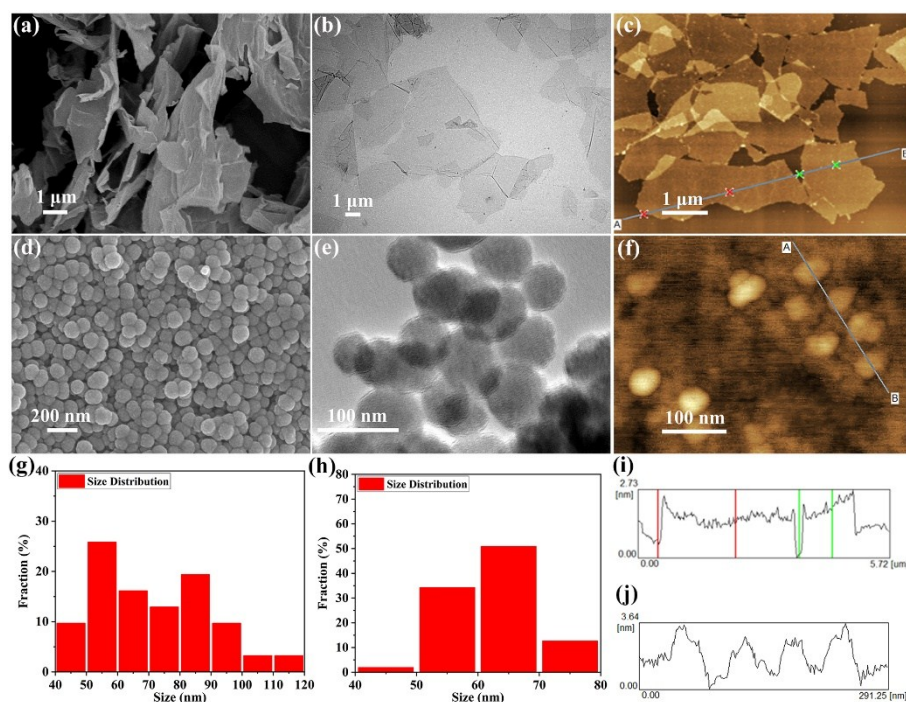


Fig. S1 SEM (a), TEM (b) and AFM (c) images of GO, and SEM (d), TEM (e) and AFM (f) images of GQDs. The size distributions of the GQDs obtained from SEM (g) and TEM (h). The corresponding height profiles along the indicated lines in AFM image of GO (i) and GQDs (j).

Fig. S2a presents the FT-IR spectra of GO and GQDs. The spectrum of GO presents characteristic peaks at 3422 cm^{-1} for -OH stretching, 1724 cm^{-1} for C=O stretching, 1619 cm^{-1} for skeletal ring vibration of the graphitic domain (C=C), 1418 cm^{-1} for -OH deformation, 1226 cm^{-1} for -C-OH stretching, and 1053 cm^{-1} for -C-O stretching, revealing that the prepared GO are rich in hydroxyl, epoxy and carboxyl groups.^{1,2} After hydrothermal treatment, peaks related to hydroxyl and epoxy groups on GO sheets were disappeared. New broad peaks at 3384 cm^{-1} and 3153 cm^{-1} for -NH₂ vibration, 1593 cm^{-1} and 1401 cm^{-1} for carboxylate (-COO⁻) and ammonium (NH₄⁺) vibrations, and 1337 cm^{-1} for C-N stretching vibration were observed in GQDs. Meanwhile, a shoulder peak attributes to carboxyl (-COOH) can also be observed before the peak at 1593 cm^{-1} , indicating the existence of the amino (-NH₂), carboxyl (-COOH) and ammonium carboxylate (-COO·NH₄⁺) groups on the GQDs.^{3,4}

As shown in Fig. S2b, the XPS survey spectrum of GO shows the predominant C1s peak at about 284 eV and an O1s peak at about 532 eV. For the spectrum of GQDs, in addition to the C1s and O1s peaks, a new N1s peak at about 400 eV was observed. The existence of N1s confirms the successful introduction of N onto the GQDs after the hydrothermal treatment. The high resolution C1s XPS spectrum of GO reveals the presence of various types of carbon bonding, such as C=C/C-C (284.5 eV), C-O (C-OH/-C-O-C-) (286.5 eV) and C=O (O=C-OH) (288.5 eV), which was consistent with the corresponding FT-IR spectrum of GO.^{5,6} For the C1s XPS spectrum of GQDs, the signal peak of C-O disappeared, and a new signal peak (285.8 eV) attributing to C-N bond was observed.⁷ Meanwhile, a signal peak (288.6 eV) assigned to C=O bond with stronger intensity compared to that of GO could be observed. The quantitative analysis (Table S1) show that the O/C atomic ratio for the GQDs is ca. 62%, higher than that of GO (ca. 44%), indicating the further oxidation of C=C during hydrothermal treatment.¹⁸ Further details of the N bonding states are presented in the high resolution N1s spectrum as shown in Fig. S2e. The N1s spectrum composed of two peaks at 399.5 eV and 401.5 eV for C-N and NH₄⁺, respectively. The presence of the C-N signal provides evidence for the success introduction of nitrogen (amino group) on the surface of GQDs rather than graphitizing the carbon cores inside of GQDs (pyridinic and pyrrolic nitrogen in the plane of graphene structure), and the presence of the NH₄⁺ signal indicates that the as-prepared GQDs contain ammonium carboxylate groups.^{3,4} Moreover, the carbon and nitrogen bonding compositions determined from the deconvolution of the C1s and N1s spectra (Table S2 and Table S3) demonstrated that the increase of -NH₂ and -COO·NH₄⁺ groups is based on the expense of all hydroxyl/epoxy and partial carboxyl groups.^{8,9} The results were also in accordance with the related observation in the FT-IR results very well.

The zeta potentials of the GQDs solution (1 mg/mL) at different pH values were also investigated. As shown in Fig. S2f, zeta potentials changed from -18.4 mV to -46.8 mV by increasing the pH value from 2 to 11. The positive shift of the zeta potential with the decrease of pH value for the GQDs solutions indirectly indicates the introduction of amino groups since the introduced amino groups can counteract part of the electronegative effect of carboxylate groups. The negative shift of zeta potential

with the increase of pH value also indirectly indicates the existence of unprotonated carboxyl groups, which is in good agreement with FT-IR and XPS results.

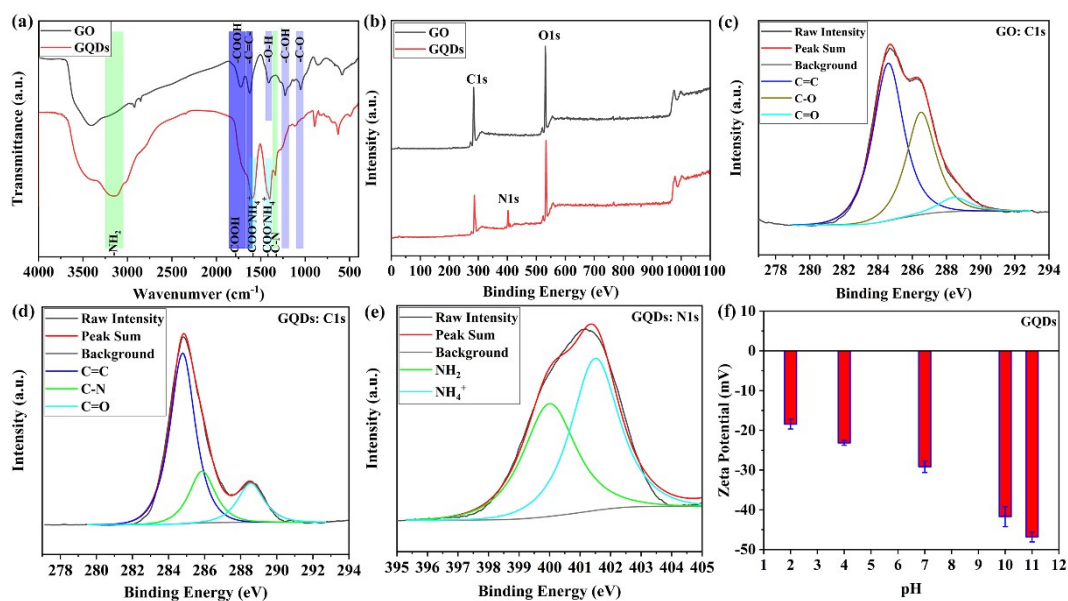


Fig. S2 FTIR spectra (a) and XPS survey spectra (b) of GO and GQDs; High-resolution XPS C1s spectra of GO (c) and GQDs (d); and high-resolution N1s spectrum of GQDs (e). Zeta potentials of GQDs solutions (1 mg/mL) at different pH values (f).

Table S1. Relative atomic percentage of chemical elements in GO and GQDs.

Sample	Relative atomic percentage (at. %)		
	C	O	N
GO	69.5	30.5	0
GQDs	55.1	34.2	10.7

Table S2. Carbon bonding composition determined from the C1s XPS.

Sample	Carbon bonding composition (%)				
	C=C	C-O (C-OH)	C=O (-COOH)	C-N (-C-NH ₂)	C=O (-COO-NH ₄ ⁺)
GO	58.2	36.5	5.3	---	---
GQDs	57.8	---	---	19.7	22.5

Table S3. Nitrogen bonding composition determined from the N1s XPS.

Sample	Nitrogen bonding composition (%)	
	-NH ₂	NH ₄ ⁺
GQDs	44.9	55.1

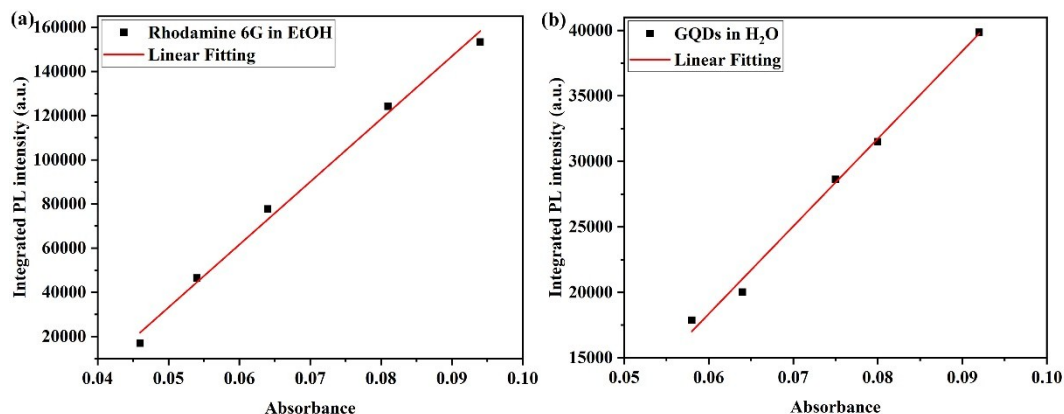


Fig. S3 Plots of integrated PL intensity of rhodamine 6G (a) and GQDs (b) as a function of optical absorbance at 450 nm.

Table S4. Integrated photoluminescence intensity and absorbance data of the rhodamine 6G and GQDs as a function of optical absorbance at 450 nm.

Sample	Rhodamine 6G	GQDs
Abs	0.046	0.058
	0.054	0.064
	0.064	0.075
	0.081	0.080
	0.094	0.092
Integrated PL	16969.027	17867.167
	46527.593	20026.712
	77748.735	28634.278
	124182.519	31509.555
	153318.026	39865.925
Slope	2841250	668925
QY	95 %	21.4 %

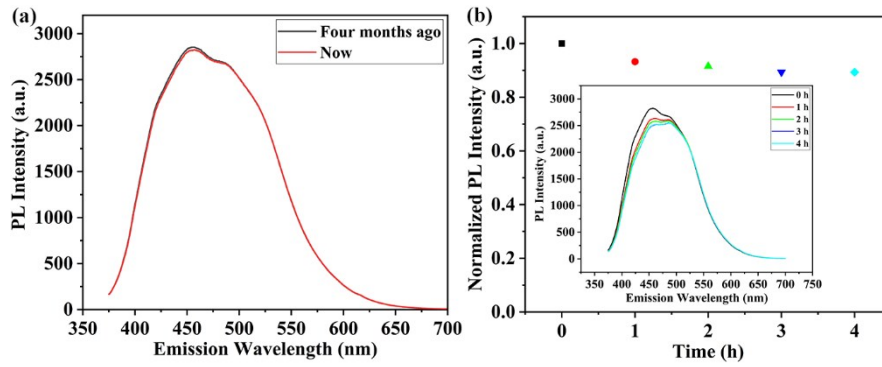


Fig. S4 (a) Comparison of PL spectra of GQDs solution after four months. (b) Effect of irradiation time with 365 nm UV light (150 W xenon lamp) on the PL intensity of GQDs. (Inset: (b) the PL spectra of GQDs solution after different irradiation time)

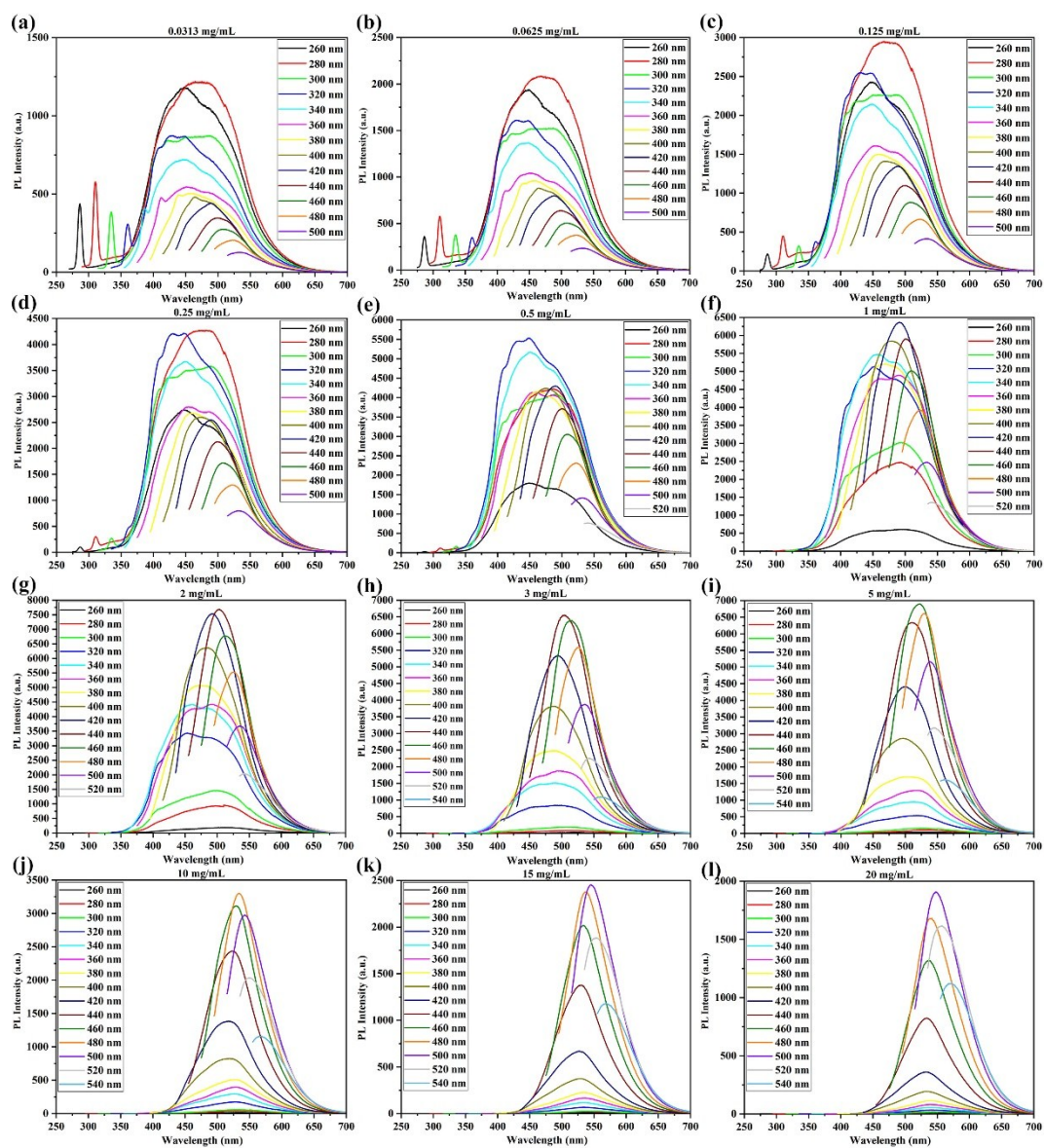


Fig. S5 PL emission spectra of GQDs solutions with different concentrations at different excitation wavelengths.

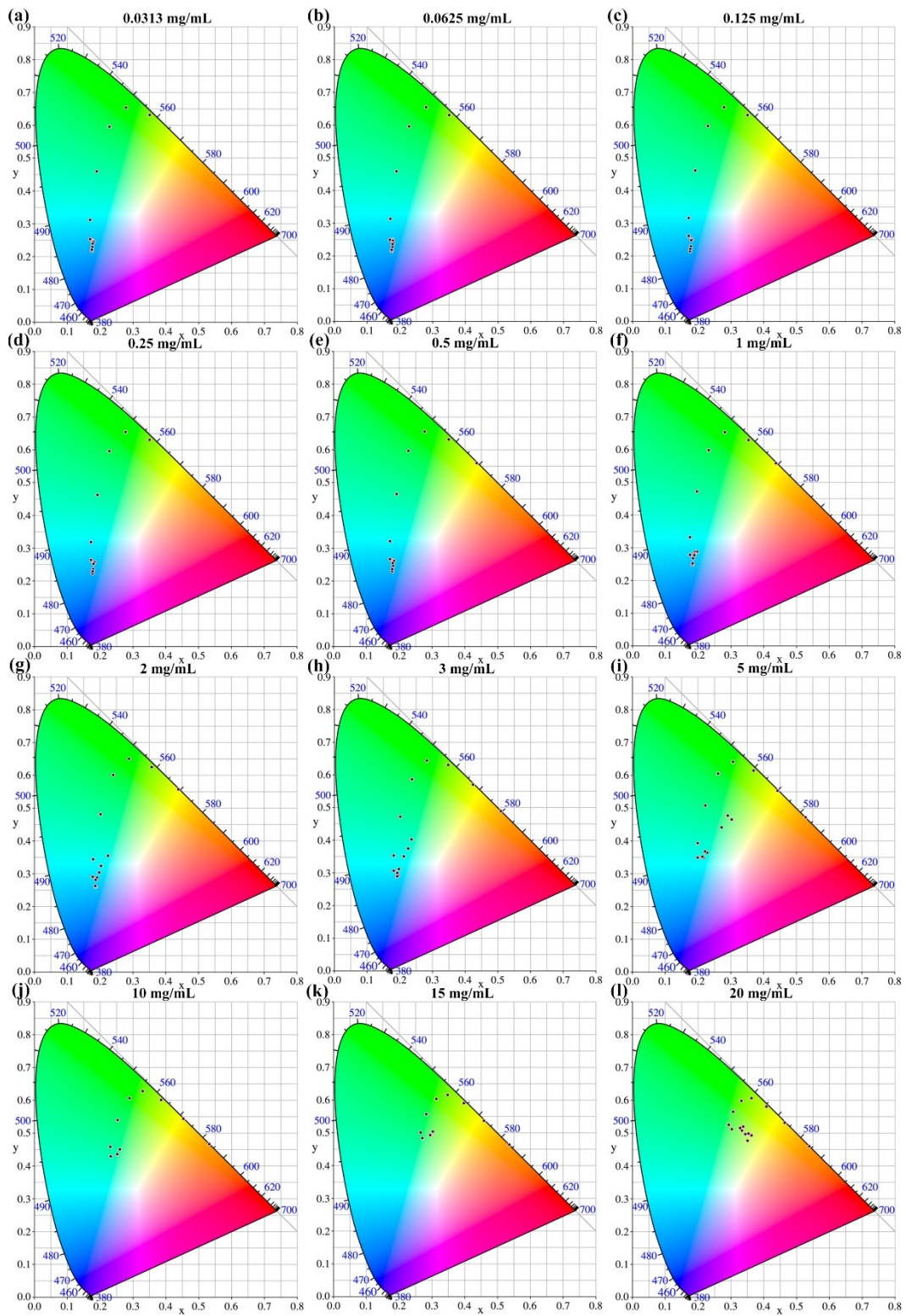


Fig. S6 Corresponding chromaticity coordinates of the GQDs aqueous solution with different concentrations upon excitation at different excitation wavelength.

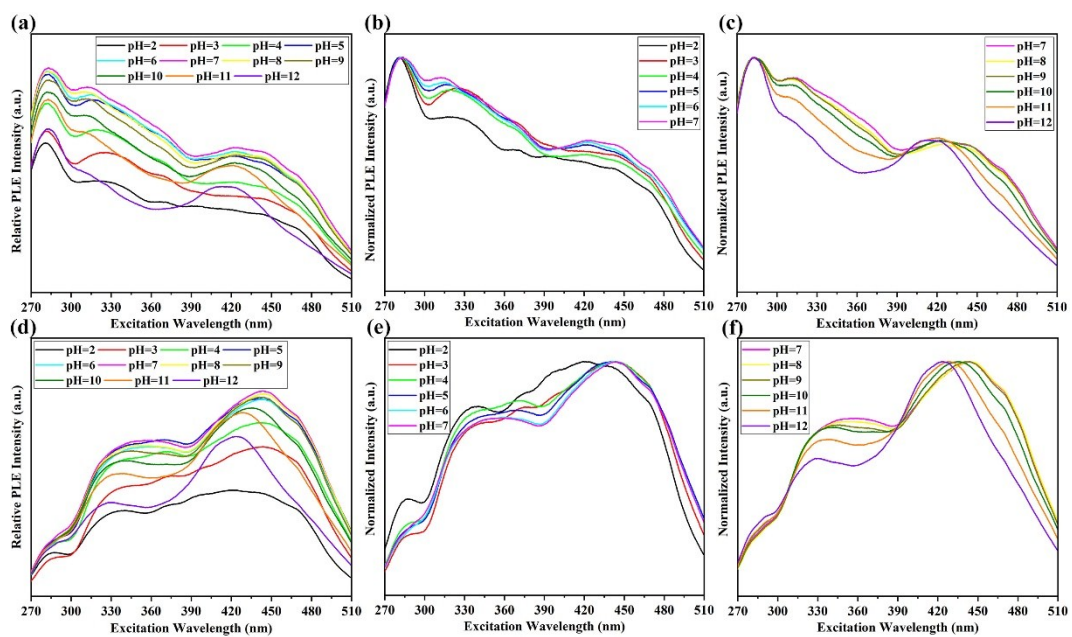


Fig. S7 PLE and normalized PLE spectra of GQDs solution with concentrations of 0.25 mg/mL ((a), (b), (c)) and 1 mg/mL ((d), (e), (f)) under different pH conditions.

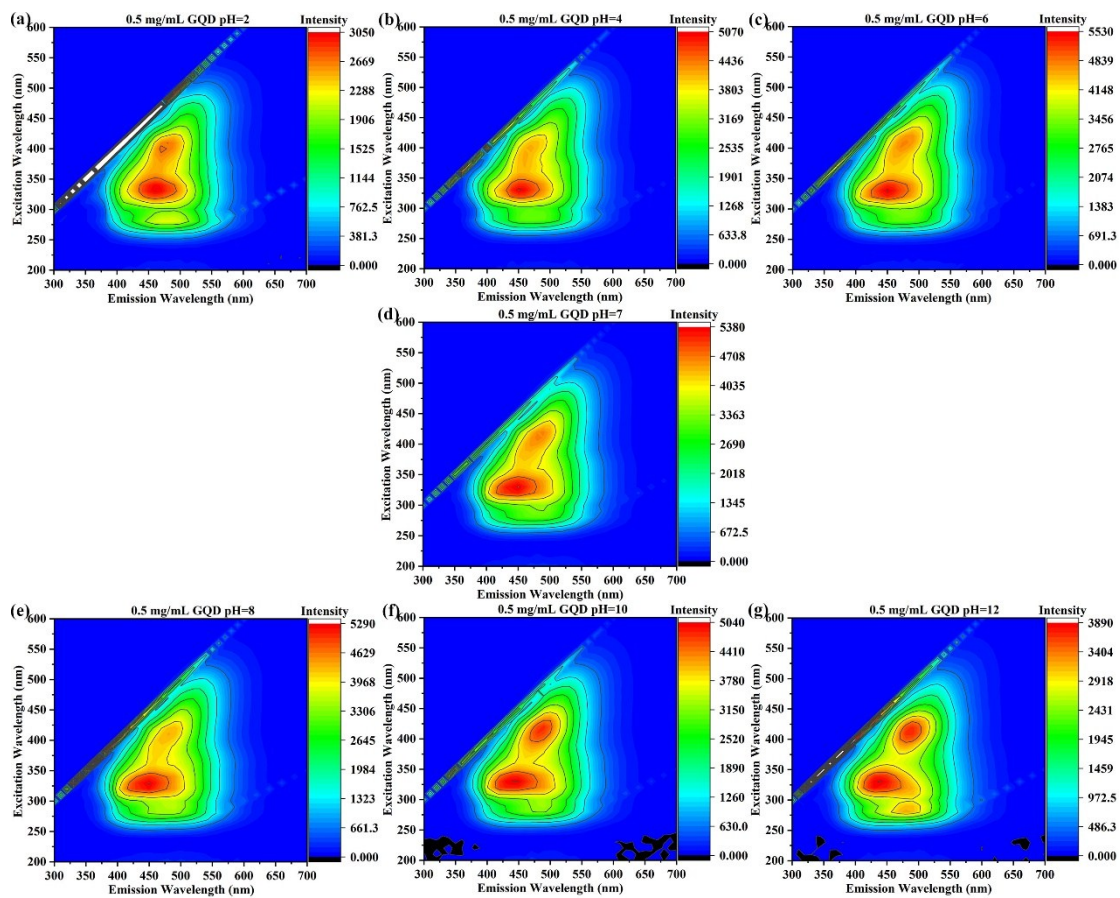


Fig. S8 3D fluorescence spectroscopy analysis of GQDs solutions (0.5 mg/mL) at different pH conditions.

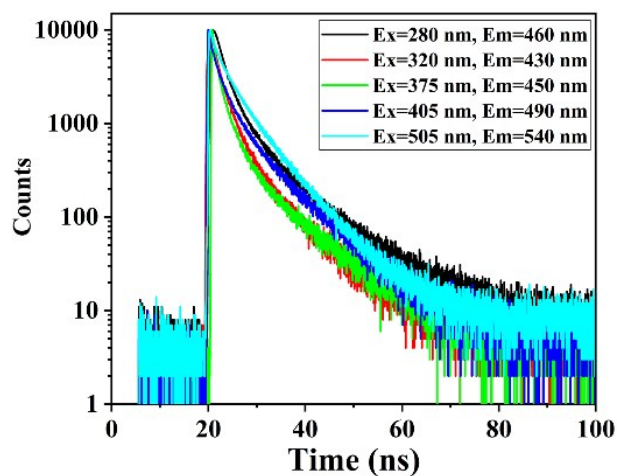


Fig. S9 Time resolved fluorescence decay traces of GQDs solution (0.125 mg/mL) at different excitation and emission wavelengths.

Table S5. PL lifetimes and amplitudes obtained from PL decay curves of GQDs at different excitation and emission wavelength.

Ex/Em	τ_{av} (ns)	τ_1 (ns): A_1 (%)	τ_2 (ns): A_2 (%)	τ_3 (ns): A_3 (%)	χ^2
280 nm/460 nm	1.76	2.83:28	1.06:5	0.68:67	1.189
320 nm/430 nm	1.59	2.40:36	8.83:4	0.61:60	1.163
375 nm/450 nm	1.17	1.95:31	9.43:4	0.32:65	1.671
405 nm/490 nm	2.15	2.45:40	8.66:11	0.46:49	1.242
505 nm/540 nm	3.28	3.11:41	7.44:24	0.63:35	1.239

τ_{av} : the average lifetime τ_{av} is given by
$$\tau_{av} = \frac{A_1\tau_1^2 + A_2\tau_2^2 + A_3\tau_3^2}{A_1\tau_1 + A_2\tau_2 + A_3\tau_3}$$
. The goodness-of-fit was determined by the χ^2 value.

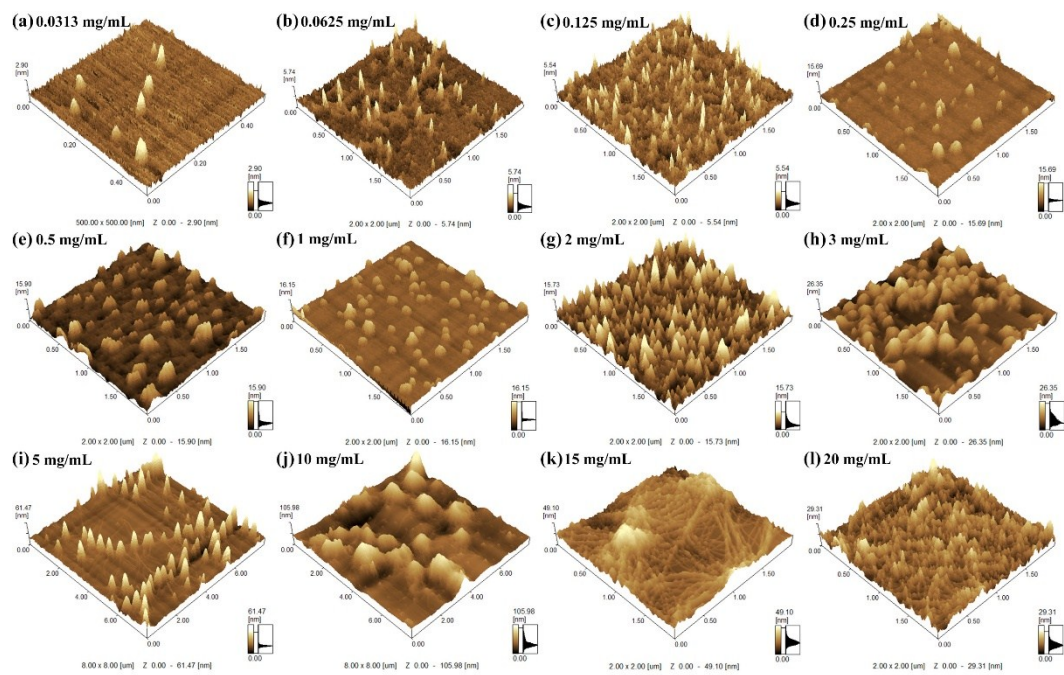


Fig. S10 Three-dimensional AFM images of GQDs solutions with different concentrations.

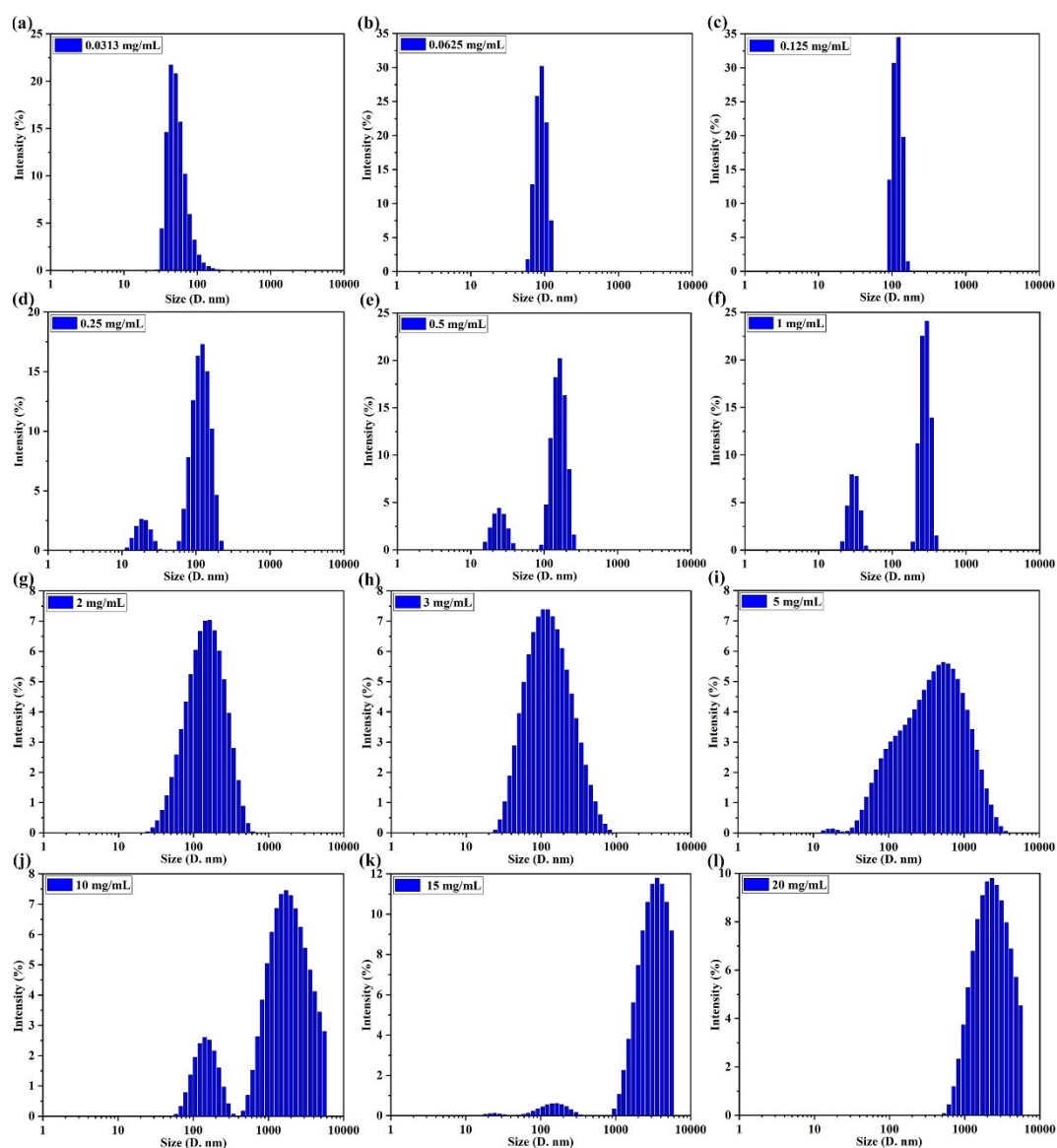


Fig. S11 Dynamic light scattering (DLS) analysis of GQDs solutions with different concentrations.

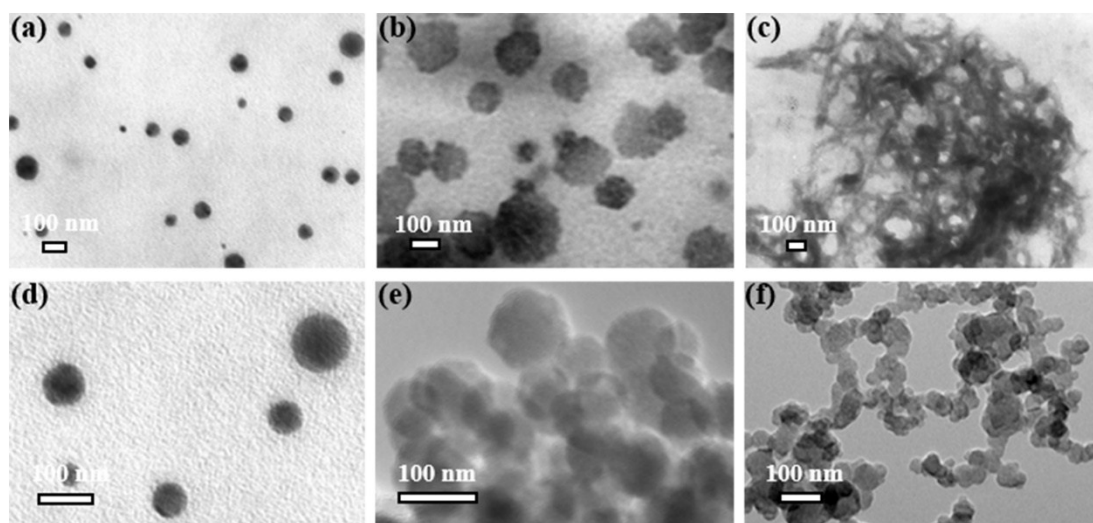


Fig. S12 TEM and enlarged TEM images of GQDs solutions with different concentrations. (a) and (d): 0.0625 mg/mL, (b) and (e): 1 mg/mL, (c) and (f): 10 mg/mL.

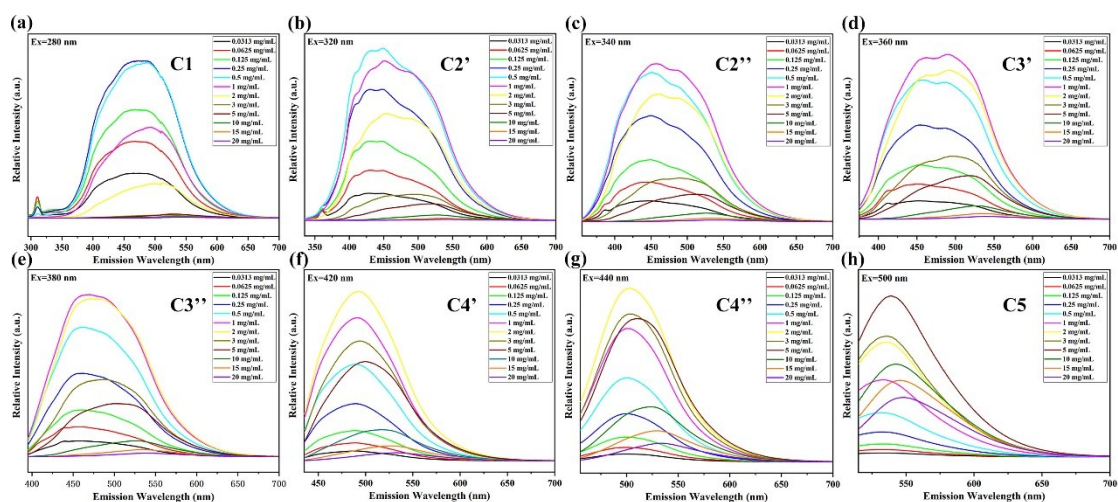


Fig. S13 PL spectra of different fluorescent centers (C1 (a), C2 (b and c), C3 (d and e), C4 (f and g), C5 (g)) in GQDs solutions with different concentrations at their corresponding excitation wavelengths.

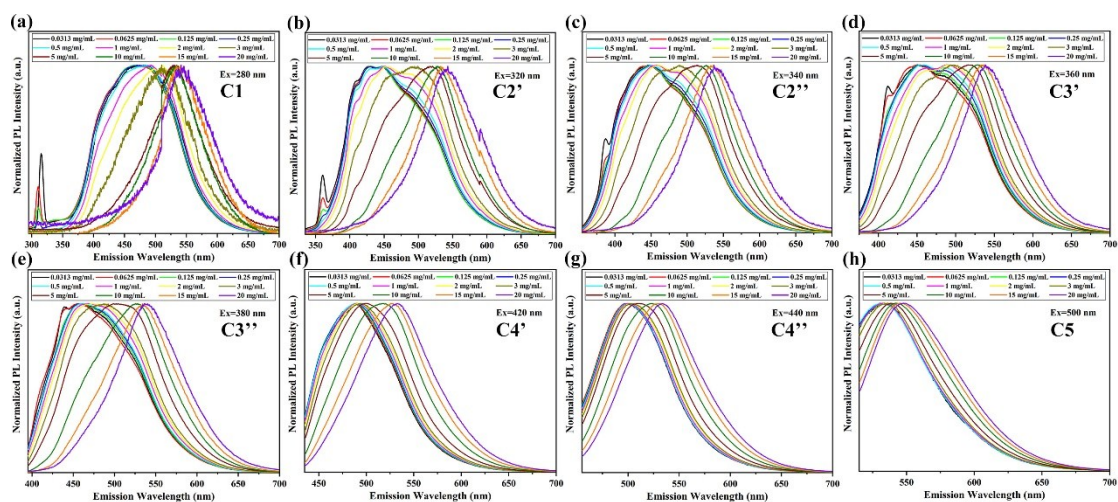


Fig. S14 Normalized PL spectra of different fluorescent centers (C1 (a), C2 (b and c), C3 (d and e), C4 (f and g), C5 (g)) in GQDs solutions with different concentrations at their corresponding excitation wavelengths.

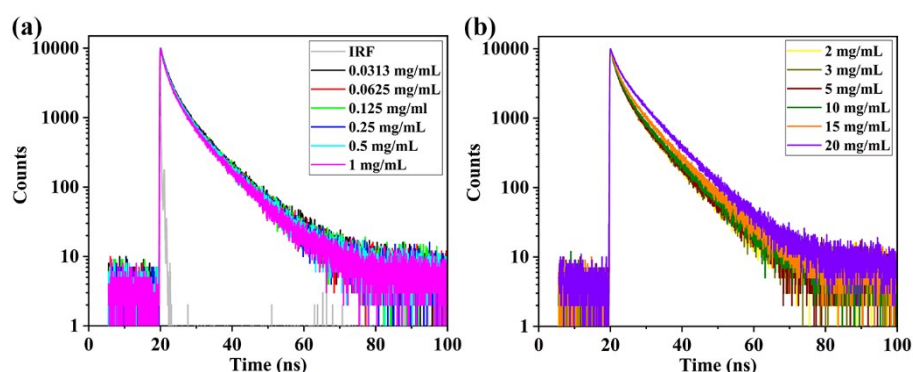


Fig. S15 Time resolved fluorescence decay traces of GQDs solutions at different concentrations (excitation wavelength: 405 nm, monitoring wavelength: 520 nm)

Table S6. PL lifetimes and amplitudes obtained from PL decay curves of GQDs solutions at different concentrations. (excitation wavelength: 405 nm, monitoring wavelength: 520 nm)

Sample	τ_{av} (ns)	τ_1 (ns): A_1 (%)	τ_2 (ns): A_2 (%)	τ_3 (ns): A_3 (%)	χ^2
0.0313 mg/mL	2.70	2.66:42	8.51:16	0.58:42	1.233
0.0625 mg/mL	2.58	2.59:42	8.30:15	0.55:43	1.175
0.125 mg/mL	2.61	2.62:42	8.49:15	0.56:43	1.224
0.25 mg/mL	2.52	2.51:43	8.29:15	0.50:42	1.253
0.5 mg/mL	2.54	2.61:41	8.34:15	0.54:44	1.185
1 mg/mL	2.45	2.55:40	8.20:14	0.57:45	1.191
2 mg/mL	2.53	2.49:41	8.25:15	0.51:43	1.132
3 mg/mL	2.53	2.56:39	8.23:16	0.55:45	1.147
5 mg/mL	2.53	2.47:39	8.13:17	0.49:44	1.256
10 mg/mL	2.64	2.46:38	8.09:19	0.47:44	1.236
15 mg/mL	3.15	2.74:36	8.21:24	0.60:41	1.162
20 mg/mL	4.10	3.31:31	8.39:33	0.80:36	1.158

References:

- 1 C. Hontorialucas, A. J. Lopezpeinado, J. D. D. Lopezgonzalez, M. L. Rojascervantes and R. M. Martinaranda, *Carbon*, 1995, **33**, 1585-1592.
- 2 S. Stankovich, R. D. Piner, S. T. Nguyen and R. S. Ruoff, *Carbon*, 2006, **44**, 3342-3347.
- 3 H. Tetsuka, R. Asahi, A. Nagoya, K. Okamoto, I. Tajima, R. Ohta and A. Okamoto, *Adv. Mater.*, 2012, **24**, 5333-5338.

- 4 F. Jiang, D. Q. Chen, R. M. Li, Y. C. Wang, G. Q. Zhang, S. M. Li, J. P. Zheng, N. Y. Huang, Y. Gu, C. R. Wang and C. Y. Shu, *Nanoscale*, 2013, **5**, 1137-1142.
- 5 J. D. Renteria, S. Ramirez, H. Malekpour, B. Alonso, A. Centeno, A. Zurutuza, A. I. Cocemasov, D. L. Nika and A. A. Balandin, *Adv. Funct. Mater.*, 2015, **25**, 4664-4672.
- 6 P. Zhang, J. L. Gong, G. M. Zeng, C. H. Deng, H. C. Yang, H. Y. Liu and S. Y. Huan, *Chem. Eng. J.*, 2017, **322**, 657-666.
- 7 C. Zhu, Y. J. Fu, C. A. Liu, Y. Liu, L. L. Hu, J. Liu, I. Bello, H. Li, N. Y. Liu, S. J. Guo, H. Huang, Y. Lifshitz, S. T. Lee and Z. H. Kang, *Adv. Mater.*, 2017, **29**, 1701399.
- 8 F. H. B. Baldovino, A. T. Quitain, N. P. Dugos, S. A. Roces, M. Koinuma, M. Yuasa and T. Kida, *Rsc. Adv.*, 2017, **7**, 3852-3852.
- 9 D. Qu, M. Zheng, L. G. Zhang, H. F. Zhao, Z. G. Xie, X. B. Jing, R. E. Haddad, H. Y. Fan and Z. C. Sun, *Sci. Rep.*, 2014, **4**, 5294.